Supplementary Materials for

Isotopic constraints on wildfire derived HONO

Jiajue Chai[1,2], Jack E. Dibb[3], Bruce E. Anderson[4], Claire Bekker[1,2], Danielle E. Blum[1,5], Eric Heim[3], Carolyn E. Jordan[4,6], Emily E. Joyce[1,2], Jackson H. Kaspari[7], Hannah Munro[3], Wendell W. Walters[1,2], and Meredith G. Hastings[1,2]

[1] Institute at Brown for Environment and Society, Brown University, Providence, RI

[2] Department of Earth, Environmental and Planetary Sciences, Brown University, Providence, RI

[3] Institute for the Study of Earth, Ocean and Space, University of New Hampshire, Durham, NH

[4] NASA Langley Research Center, Hampton, VA

[5] Department of Chemistry, Brown University, Providence, RI

[6] National Institute of Aerospace, Hampton, VA

[7] Department of Chemistry, University of New Hampshire, Durham, NH

Correspondence to: Jiajue Chai (jiajue_chai@brown.edu)

This PDF file includes:

Figures. S1 to S5

Tables S1 to S4

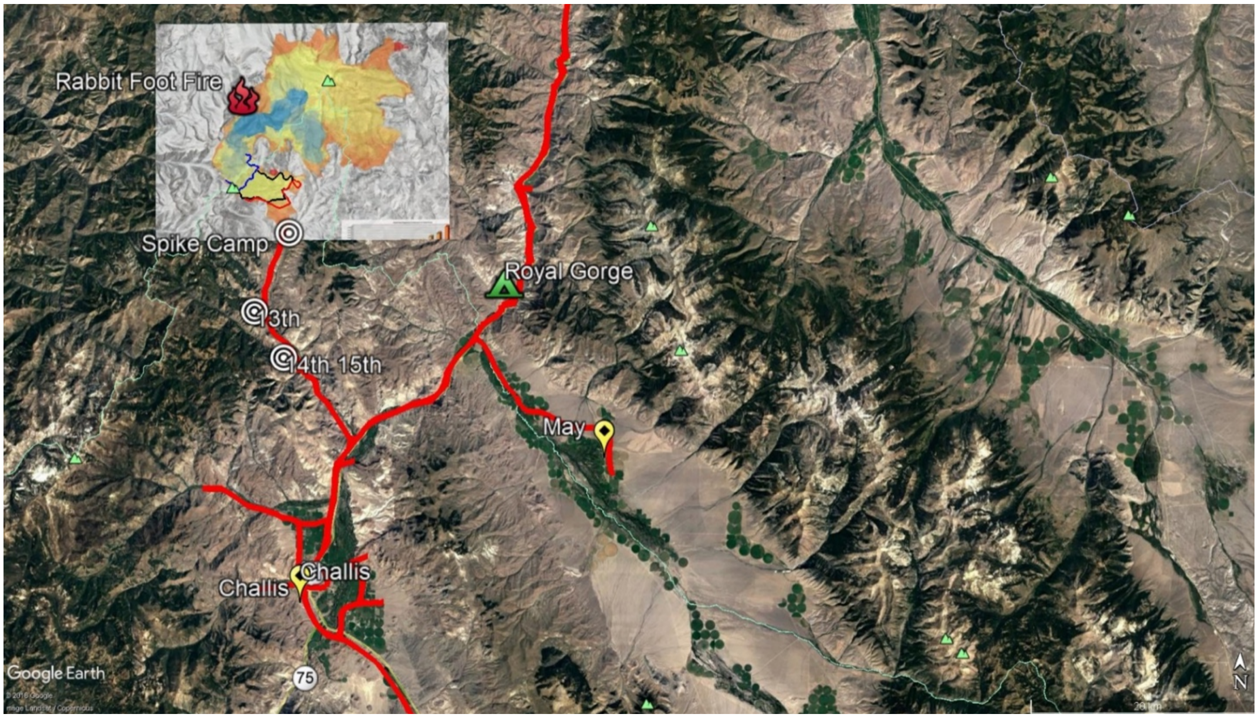

Figure S1. WE-CAN 2018 sampling map for Rabbit Foot fire (RF) in the Challis area of Salmon-Challis National Forest in central Idaho, from August 9th to August 18th 2018. Of note are important dates, which give the locations of the different approaches to the RFF during mobile measurements up MCR (H. Munro, "An Investigation of Nitrous and Nitric Acid Diurnal Cycles in Biomass Burning Plumes", Thesis, University of New Hampshire, Durham, NH, 2019).

Figure S2. Driving map during FIREX-AQ. From Jul 24 to Aug 22 of 2019, we sampled smoke from five different fires including Shady fire (Idaho), Black Diamond fire (Montana), Williams Flats fire (Washington), Nethker fire (Idaho), and Little Bear fire (Utah).

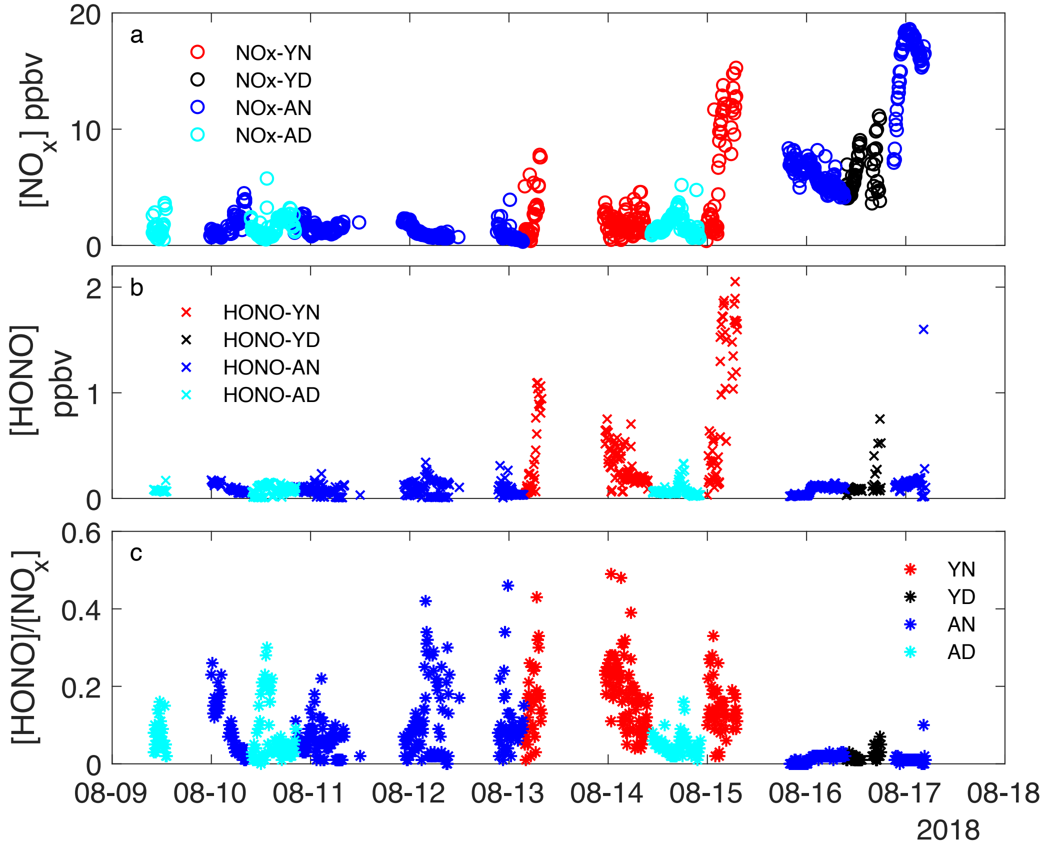

Figure S3. Time history of HONO/NO_x during WE-CAN 2018 sampling.

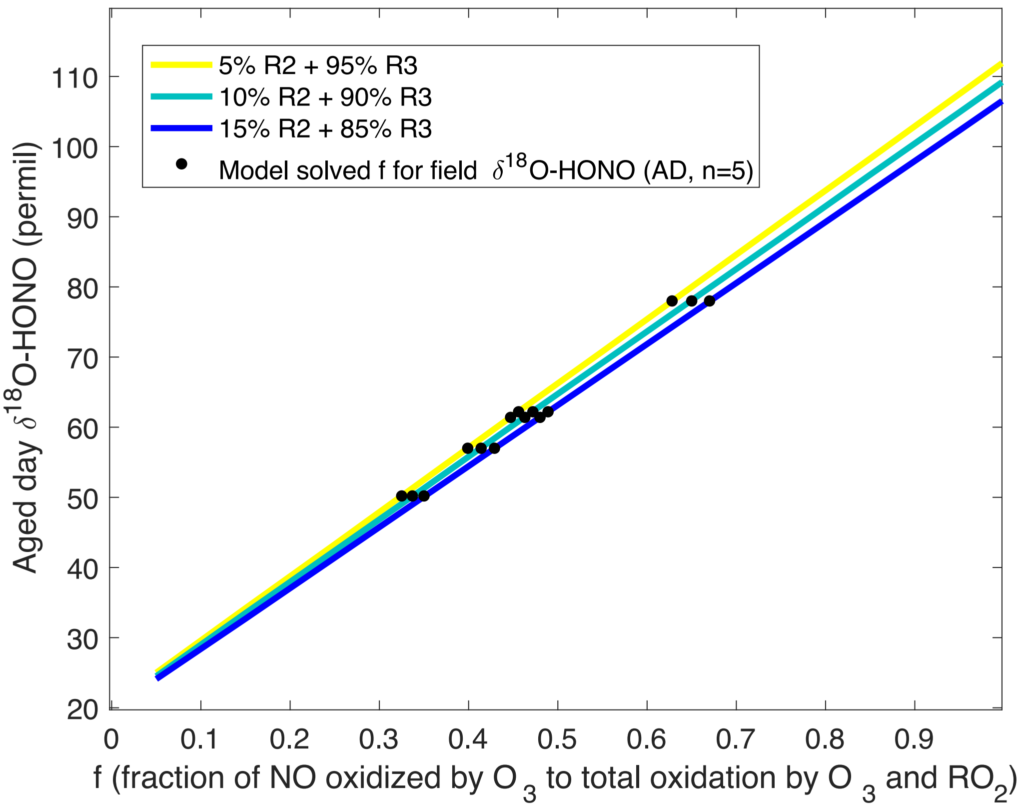

Figure S4. Modeling results for δ^{18}O-HONO in aged daytime smoke as a function of fraction of NO oxidized to NO_2 via O_3 to that via O_3 and RO_2 together ($f^{NO}_{O3/(O3+RO2)}$). The contribution of R2 to HONO production is varied from 5% to 15% following M1 in Fig. 4, and R3 accounts for the remaining secondary HONO contribution.

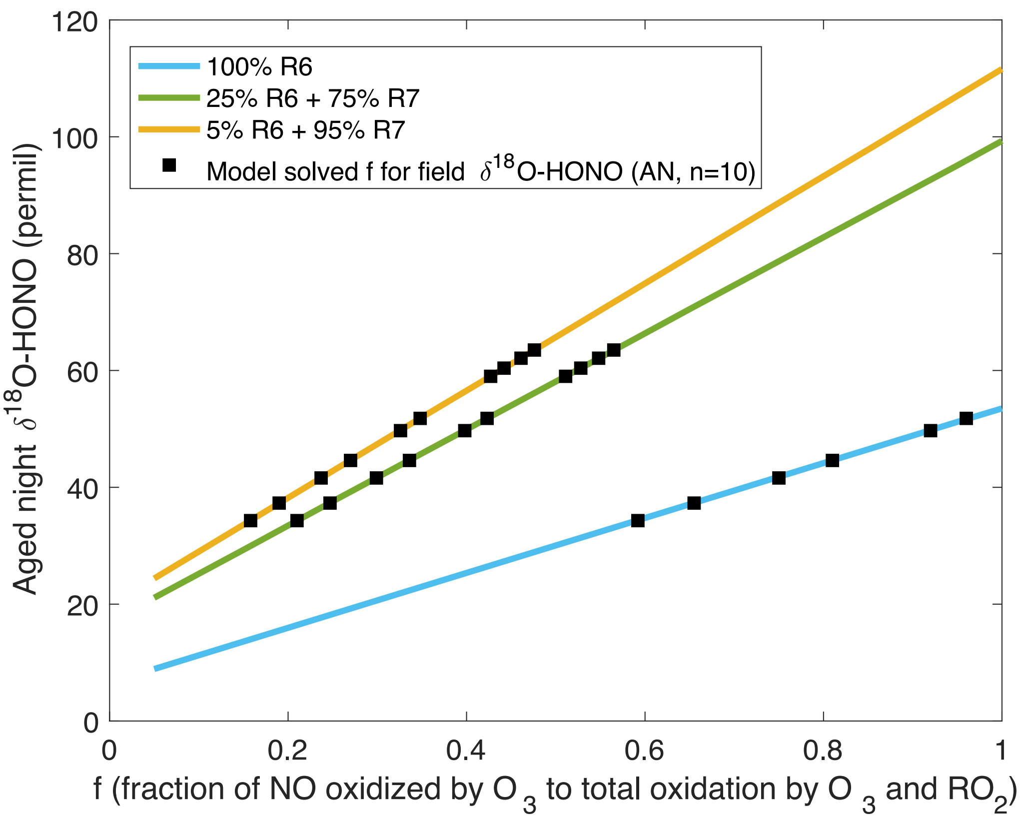

Figure S5. Modeling results for δ^{18}O-HONO in aged nighttime smoke as a function of fraction of NO oxidized to NO_2 via O_3 to that via O_3 and RO_2 together ($f^{NO}_{O3/(O3+RO2)}$). Three scenarios with various contributions of R6 and R7 are modeled. Black squares are model solved $f^{NO}_{O3/(O3+RO2)}$ to each field-observed δ^{18}O-HONO under this condition.

Table S1. Secondary formation and sink reactions and their isotopic enrichment factors for ^{15}N and ^{18}O ($^{15}\varepsilon$ and $^{18}\varepsilon$) estimated in this work.

Condition	Reaction	$^{15}\varepsilon$ ‰	$^{18}\varepsilon$ ‰
day	NO + OH —> HONO	+10	+15
day	HONO + hv —> NO + OH (λ<400 nm)	-2.5	-3.5
day	HONO + OH —> NO_2 + H_2O	N/A	N/A
day	HNO_3/NO_3^- + hv —>HONO + NOx	≤-47.9	6 to 13
day	organics + H_2O +NO_2 + hv	-2.9 to -4.5	-5.7 to -8.9
night	HONO (g) —> HONO (ads)	-2	-4
night	$2NO_2$ + H_2O —> HNO_3 + HONO	-2.9 to -4.5	-5.7 to -8.9
night	NO_2 + H_2O + Fe_xO_y (and/or quinone)	-2.9 to -4.5	-5.7 to -8.9

Table S2. Rate coefficients used in this work (Burkholder et al. 2019[a])

Reaction	Rate coefficient (298 K) $cm^3\ s^{-1}$
HO_2 + NO —> OH + NO_2	8.0×10^{-12}
NO + O_3 —> NO_2 + O_2	1.9×10^{-14}
$C_2H_5O_2$ + NO —> product	8.7×10^{-12}
CH_3O_2 + NO —> CH_3O + NO_2	7.7×10^{-12}
RO_2 + NO —> product	8.0×10^{-12}
RO_2 + NO —> $RONO_2$	3.2×10^{-13}

[a] Burkholder, J. B., Sander, S. P., Abbatt, J., Barker, J. R., Cappa, C., Crounse, J. D., Dibble, T. S., Huie, R. E., Kolb, C. E., Kurylo, M. J., Orkin, V. L., Percival, C. J., Wilmouth, D. M. and Wine P. H.: "Chemical Kinetics and Photochemical Data for Use in Atmospheric Studies, Evaluation No. 19," JPL Publication 19-5, Jet Propulsion Laboratory, Pasadena, 2019.

Table S3. Modeling results for $\Delta\delta^{15}N_{HONO\text{-}NOx}$ (‰).

Remaining HONO	$\Delta\delta^{15}N_{HONO\text{-}NOx}$ (5%R2+95%R3)	$\Delta\delta^{15}N_{HONO\text{-}NOx}$ (10%R2+90%R3)	$\Delta\delta^{15}N_{HONO\text{-}NOx}$ (15%R2+85%R3)	$\Delta\delta^{15}N_{HONO\text{-}NOx}$ (10%R2+85%R3 +5%R4)	$\Delta\delta^{15}N_{HONO\text{-}NOx}$ (10%R2+80%R3 +10%R4)	$\Delta\delta^{15}N_{HONO\text{-}NOx}$ (10%R2+75%R3 +15%R4)
0.9	-1.8	-1.2	-0.5	-3.4	-5.6	-7.8
0.8	-1.6	-0.9	-0.3	-3.1	-5.3	-7.5
0.7	-1.3	-0.6	0.0	-2.8	-5.0	-7.2
0.6	-0.9	-0.3	0.4	-2.5	-4.7	-6.9
0.5	-0.5	0.1	0.8	-2.1	-4.3	-6.5
0.4	0.0	0.7	1.3	-1.5	-3.7	-5.9
0.36	0.2	0.9	1.5	-1.3	-3.5	-5.7
0.32	0.5	1.2	1.8	-1.0	-3.2	-5.4
0.28	0.8	1.5	2.1	-0.7	-2.9	-5.1
0.24	1.2	1.8	2.5	-0.4	-2.6	-4.8
0.2	1.6	2.2	2.9	0.0	-2.2	-4.4
0.16	2.1	2.8	3.4	0.6	-1.6	-3.8
0.12	2.8	3.4	4.1	1.2	-1.0	-3.2
0.08	3.7	4.3	5.0	2.1	-0.1	-2.3
0.04	5.3	5.9	6.6	3.7	1.5	-0.7
0.02	6.8	7.5	8.1	5.3	3.1	0.9

Table S4. Modeling results for $\delta^{18}O$ aged daytime and aged nighttime (‰).

$k_{O3}[O_3]/k_{RO2}[RO_2]+k_{O3}[O_3]$	Day			Night		
	$\delta^{18}O$-HONO (5%R2+95%R3)	$\delta^{18}O$-HONO (10%R2+90%R3)	$\delta^{18}O$-HONO (15%R2+95%R3)	$\delta^{18}O$-HONO (100%R6)	$\delta^{18}O$-HONO (25%R6+75%R7)	$\delta^{18}O$-HONO (5%R6+95%R7)
0.05	25.0	24.5	24.1	8.9	21.1	24.4
0.15	34.2	33.5	32.7	13.6	29.3	33.6
0.25	43.3	42.4	41.4	18.3	37.6	42.8
0.35	52.5	51.3	50.1	23.0	45.8	52.0
0.429	59.8	58.4	57.0	26.7	52.3	59.2
0.592	74.7	72.9	71.2	34.3	65.7	74.2
0.65	80.0	78.1	76.2	37.1	70.5	79.5
0.75	89.2	87.0	84.9	41.8	78.7	88.7
0.85	98.3	96.0	93.6	46.5	86.9	97.8
0.95	107.5	104.9	102.3	51.2	95.1	107.0
1	112.1	109.4	106.7	53.5	99.3	111.6